Panel Adjustment and Error Analysis for a Large Active Main Reflector Antenna by Using the Panel Adjustment Matrix

Peiyuan Lian, Congsi Wang, Song Xue, Qian Xu, Na Wang, Binbin Xiang, Yu Shi, and Yu Jia

Abstract—**Active panels are generally applied in large aperture and high frequency reflector antennas, and the precise calculation of the actuator adjustment value is of great importance. First, the approximation relationship between the adjustment value and panel elastic deformation is established. Subsequently, a panel adjustment matrix for the whole reflector is derived to calculate the reflector deformation caused by the actuator adjustment. Next, the root mean square (rms) error of the deformed reflector is expressed as a quadratic form in the matrix form, and the adjustment value can be derived easily and promptly from the corresponding extreme value. The solution is expected to be unique and optimal since the aforementioned quadratic form is a convex function. Finally, a 35 m reflector antenna is adopted to perform the panel adjustments, and the effect of the adjustment errors is discussed. The results show that compared to the traditional model, where the panel elastic deformation is not considered, the proposed method exhibits a higher accuracy and is more suitable for use in large reflectors with a high operation frequency. The adjustment errors in different rings exert different influences on the gain and sidelobe level, which can help determine the actuator distribution with different precisions.**

Index Terms—**Panel Adjustment Matrix, Active Panel, Error Analysis, Power Pattern, Reflector Antenna**

I. INTRODUCTION

Large reflector antennas have been widely used in deep space exploration, radio astronomy, communications, and other applications, owing to their simple structure, high gain, and narrow beam [1]-[2]. With the development of reflector antennas to have large apertures and high frequencies, such

P.Y. Lian, C.S. Wang, and S. Xue are with the School of Electromechanical Engineering, Xidian University, Xi'an, No. 2 Taibai South Road 710071, China. (lian100fen@126.com, congsiwang@163.com,sxue@xidian.edu.cn).

Q. Xu, N. Wang, and B.B. Xiang are with the Xinjiang Astronomical Observation, Chinese Academy of Sciences, Urumqi 830011, China. (xuqian@xao.ac.cn, na.wang@xao.ac.cn, xiangbinbin@xao.ac.cn).

Y. Shi is with the Department of Mechanical Engineering, University of Chester, Chester, CH2 4NU, UK. (y.shi@chester.ac.uk)

Y. Jia is with the Department of Mechanical Engineering, Aston University, Birmingham, B4 7ET, UK. (yu.jia.gb@ieee.org)

antennas must operate in the open air due to their large apertures and are thus inevitably affected by external loads such as gravity, temperature, and wind. In such cases, the reflector may be deformed, leading to a considerable deterioration in its electromagnetic (EM) performance [3]-[6]. Moreover, owing to the high frequency, a high surface precision must be ensured, which notably increases the difficulty in the structure design [7]-[8]. To ensure high surface precision, active main reflectors with adjustable panels have been widely applied to large reflector antennas operating in the millimeter or submillimeter wave band [9]-[10], such as the 110 m Green Bank telescope with 2004 panels supported by 2209 actuators, and the 65 m Tianma telescope with 1008 panels and 1104 actuators. As shown in Fig. 1, each panel of the active main reflector is supported by four actuators and can be adjusted to the locations of the ideal reflector or best fitting reflector. Thus, the deformation measurement and panel adjustment calculation of the deformed reflector are two particularly important research areas [11]-[13]. However, in this paper, we focus on the panel adjustment calculation and the effect analysis of the panel adjustment error on the EM performance of the reflector.
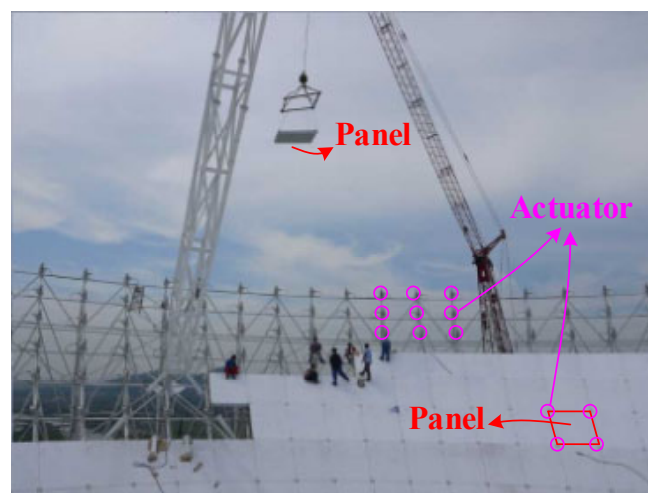

Fig. 1. Active main reflector of the 65-m Tianma telescope in China.

Reflector deformation compensation has been discussed in many papers. Two compensation methods are commonly applied. The first approach involves moving the subreflector for the nonactive main reflector antenna through one six bar mechanism, and the second approach is to adjust the panels for

the active main reflector antenna through thousands of actuators [14]. Reference [15] presented a subreflector adjustment method to compensate for the main reflector deformation through the surface piecewise fitting of the deformed main reflector. References [16] and [17] indicated that the main reflector surface accuracy can be enhanced to a certain extent by moving the subreflector to a new location determined based on the best fitting reflector. However, the best fitting error of the deformed main reflector cannot be compensated for by moving subreflector. For the active main reflector antenna, the reflector deformation can be well compensated by adjusting thousands of actuators. Reference [18] described a calculation process of the panel adjustment; however, only the best fitting reflector was considered, and the panel elastic deformation was not taken into account. In [19], the panel adjustment was discussed; however, the method pertained only to the panel installation procedure, and the panel was approximated as a rigid body with no elastic deformation. In [20], a novel application for the active surface of a shaped reflector for the primary focus operation was presented, and satisfactory results were obtained; however, the actuators were adjusted only to the positions of the panel vertices of the best fitting reflector, and the panel elastic deformation was not considered. In [21], a panel mold sharing design was adopted to reduce the cost; however, the panel adjustment was not considered. Overall, although panel adjustment has been examined in many studies, the research on the detailed adjustment calculation procedure for the active main reflector with thousands of actuators is lacking. The common limitation is that the panel elastic deformation is not considered, owing to which, the derived adjustment is not optimal.

Many researches have focused on the error effect analysis of the reflector antenna considering the EM performance. In [22] and [23], the effects of random surface errors on axisymmetric and offset cylindrical reflector antennas were discussed, respectively. In [24], a practical approach was proposed to evaluate the effects of the panel manufacturing errors on the EM performance by considering the panel forms. In [25], the effects of nonuniform surface errors along the radius on the radiation characteristics of the reflector were examined, and the performance of the deformed reflector was evaluated. In [26], the influence of the buckled deformation caused by the temperature load was addressed. In [27] and [28], an interval analysis method was incorporated in the estimation of the average pattern behavior of a reflector antenna with interval surface deformations and bump-like surface deformations, respectively, and the Monte Carlo method was adopted to verify the proposed methods. Moreover, the interval analysis method is an effective analysis tool to address the uncertain-but-bounded error and has been widely applied to the tolerance analysis of array antennas [29], [30]. Different approximation calculation methods for the power pattern were proposed in [31], [32], and [33], and the effects of different external loads on the EM performance were discussed in [34], [35], and [36]. In addition, many studies were also focused on the surface error analysis, which were not listed here due to the limited space. Nevertheless, there are few researchers focused on the effect analysis of the actuator adjustment error for the active main reflector antenna considering the EM performance.

In engineering applications, the actuator adjustment value is generally determined through the deviation of the panel from the ideal reflector or best fitting reflector. Although the EM performance can be enhanced using the abovementioned traditional adjustment method, certain adjustment errors remain because the panel elastic deformation is not considered. In this paper, a more precise calculation process for the actuator adjustment value is proposed, and the effect of the actuator adjustment error on the EM performance is analyzed considering the panel elastic deformation. First, a panel adjustment matrix is derived to calculate the reflector deformations caused by all the actuators. Subsequently, the calculation of the adjustment value is transformed into a convex optimization problem, and a unique and optimal solution is derived. Based on the derived panel adjustment matrix, the adjustment error analysis is presented, and several numerical examples are considered to demonstrate the effectiveness of the proposed method and some useful results are obtained. Because the objective of the proposed method is to increase the surface accuracy by adjusting a large number of actuators when the reflector is deformed due to the external loads, the kind of loads that cause the deformation is not relevant. Moreover, because no real wind field and temperature field is available for the adopted reflector antenna to calculate the deformation, only the gravity is considered in the simulations described in this paper.

II. POWER PATTERN CALCULATION

Fig. 2 shows the geometry of a prime focus reflector antenna with a diameter D and focal length F. $D = 2a$, where a is the radius. σ is the projected circular region of the curved reflector surface on the aperture plane with the polar coordinates ρ' and ϕ'. $\hat{r}$ is the unit vector in the observation direction, and the coordinates (r, θ, ϕ) correspond to the observation point. r' corresponds the point on the reflector surface. Considering the relationship between the aperture field and far field to be a Fourier transform pair, the far field pattern can be derived as follows:

$$E(\theta, \phi) = \iint_\sigma Q(\rho') e^{jk\rho' \sin\theta \cos(\phi - \phi')} d\sigma, \qquad (1)$$

$$Q(\rho') = B + C \left(1 - \frac{\rho'^2}{a^2}\right)^P, \qquad (2)$$

where $j = \sqrt{-1}$, $k = 2\pi/\lambda$, λ is the wavelength, $Q(\rho')$ is the aperture amplitude distribution, $B + C = 1$, $1 \le P \le 2$, and the edge taper $ET = 20\log B$.
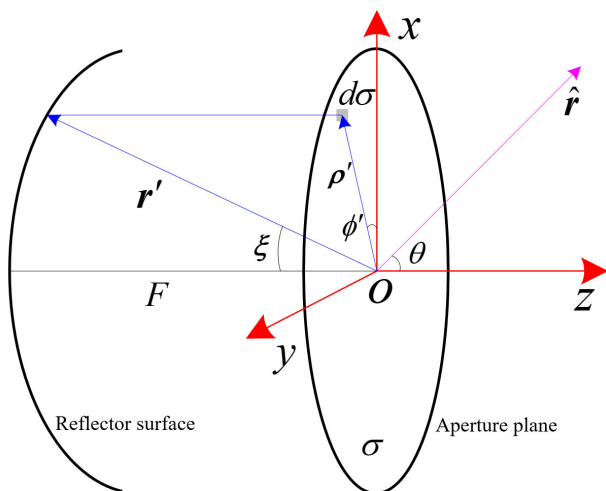
This article has been accepted for publication in a future issue of this journal, but has not been fully edited. Content may change prior to final publication. Citation information: DOI 10.1109/TAP.2021.3069493, IEEE Transactions on Antennas and Propagation

The final version is available at http://dx.doi.org/10.1109/TAP.2021.3069493

Fig. 2. Geometry of a prime focus reflector antenna.

Assuming that the reflector deformation caused by the external loads is $d(r')$, which is relative to the ideal reflector or best fitting reflector, and the reflector deformation caused by the actuator adjustment is $\delta(r')$, the total deformation Δ can be expressed as

$$\Delta(r') = d(r') + \delta(r').\qquad(3)$$

By incorporating the effect on the aperture field caused by (3) into (1), the far field pattern after the panel adjustment can be rewritten as

$$E(\theta,\varphi) = \iint_\sigma Q(\rho')\mathrm{e}^{\mathrm{j}k\rho'\sin\theta\cos(\varphi-\phi')}\mathrm{e}^{\mathrm{j}k\Delta p(\rho',\phi')}d\sigma,\quad(4)$$

where Δp is the change in the optical path length caused by the total deformation Δ in (3). The surface errors manifest in the pattern degradation primarily due to the introduction of the phase error in the reflector aperture [22], as demonstrated in [31] through formulation derivation. Thus, the surface deformation is supposed to have a negligible effect on the amplitude of the far-field pattern [27]. Δp in (4) can be expressed as $\Delta p = 2(\Delta x \cos\alpha + \Delta y \cos\beta + \Delta z \cos\gamma)\cos\gamma$, in which Δx, Δy and Δz represent the components of the total deformation Δ in the directions of the x axis, y axis, and z axis, respectively, and $\cos\alpha$, $\cos\beta$, and $\cos\gamma$ are the direction cosines of the unit normal vector of the reflector surface with $\cos\alpha = \cos\phi'$, $\cos\beta = \sin\phi'$, and $\cos\gamma = \cos(\xi/2)$.

To improve the EM performance of the deformed reflector, the total deformation Δ should be as close to zero as possible. Thus, to derive the optimal adjustment values of all the actuators, it is necessary to establish the relationship between the reflector deformation $\delta(r')$ and actuator adjustment value, as discussed in the following section.

III. Panel Adjustment Matrix

Fig. 3 shows the finite element model of the eth panel of an active main reflector antenna. The panel is supported by four actuators and reinforced by several beam structures. δ_1^e, δ_2^e, δ_3^e, and δ_4^e express the adjustment values of the four actuators, and the subscript e denotes the quantities associated with the eth panel. To derive the relationship between the deformation and all the actuators for the entire reflector, the corresponding relationship for one active panel should be first established.
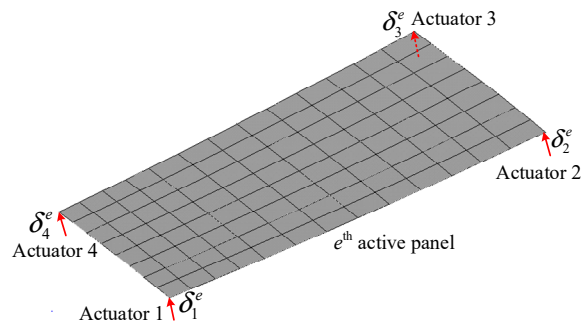

Fig. 3. Finite element model for one panel.

In Fig. 3, let δ_1^e equal 1 and δ_2^e, δ_3^e, and δ_4^e equal zero in units of millimeters. The aforementioned boundary condition is applied to the finite element model of the eth panel, and the corresponding deformation function $f_1^e(r')$ is obtained through the mechanical simulation. $\delta_1^e = 1$ indicates that the unit displacement occurs in the panel's normal direction because the actuator is generally mounted vertically to the panel. This simulation is repeated three times for $\delta_2^e = 1$, $\delta_3^e = 1$, and $\delta_4^e = 1$, and the corresponding deformation functions $f_2^e(r')$, $f_3^e(r')$, and $f_4^e(r')$ can be derived, respectively. The panel deformation depends on the four actuator adjustment values of each panel. The size of one panel generally ranges from 2 m to 5 m, and the panel maximum deformation is generally a few millimeters. Thus, the panel deformation caused by the actuators can likely be approximated through the linear superposition of the four deformation functions $f_1^e(r')$, $f_2^e(r')$, $f_3^e(r')$, and $f_4^e(r')$ with the corresponding adjustment values considered as the weights because the reflector deformation is extremely small compared with the panel size. Nevertheless, the simulation results show that the approximation error is slightly large when the four actuator adjustment values are all positive or negative due to the panel elastic deformation. Let the four actuators be displaced by 1 mm simultaneously. The fifth deformation function $f_5^e(r')$ can be derived through mechanical simulation and applied to reduce the approximation error. To simplify the formulation derivation, $f_1^e(r')$, $f_2^e(r')$, $f_3^e(r')$, $f_4^e(r')$, and $f_5^e(r')$ are replaced by $f_1^e, f_2^e, f_3^e, f_4^e$, and f_5^e, respectively.

Figs. 4(a) and 4(b) present the axial components of the deformation functions f_3^e and f_5^e, respectively. The displacement of the point inside the panel is related to the

distance between this point and the actuator; however, a certain degree of nonlinearity exists due to the panel elastic deformation. When the four actuators of one panel undergo a unit displacement simultaneously, the panel does not translate as a rigid body due to the different normal directions for these four actuators, which results in the elastic deformation.
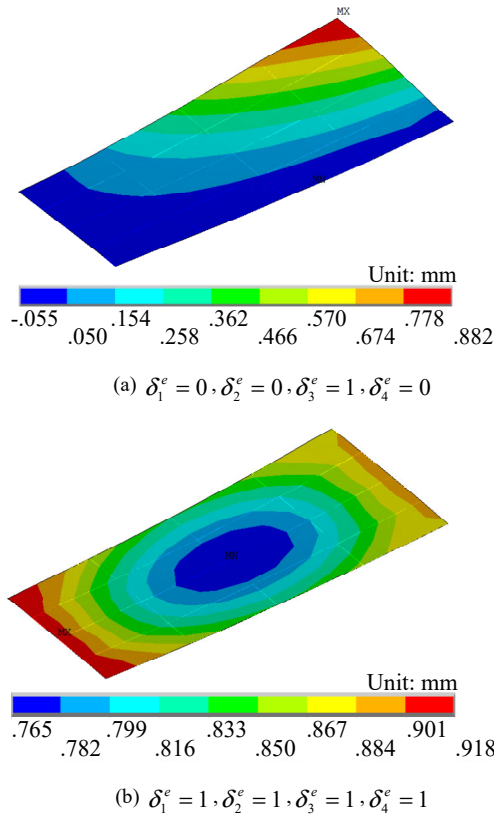

Unit: mm

-.055 .050 .154 .258 .362 .466 .570 .674 .778 .882

(a) $\delta_1^e = 0$, $\delta_2^e = 0$, $\delta_3^e = 1$, $\delta_4^e = 0$

Unit: mm

.765 .782 .799 .816 .833 .850 .867 .884 .901 .918

(b) $\delta_1^e = 1$, $\delta_2^e = 1$, $\delta_3^e = 1$, $\delta_4^e = 1$

Fig. 4. The axial components of the panel deformations

The aforementioned five functions f_1^e, f_2^e, f_3^e, f_4^e, and f_5^e are adopted as a set of basis functions to approximately calculate the panel deformation caused by the adjustment of the four actuators of the eth panel. Generally, the actuator adjustment value is small due to the small surface deformation. Therefore, to a certain extent, the corresponding panel deformation caused by the actuators can be approximated as the sum of f_1^e, f_2^e, f_3^e, and f_4^e with weights of δ_1^e, δ_2^e, δ_3^e, and δ_4^e, respectively. To improve the approximation accuracy, the fifth function f_5^e is introduced and its weight is defined as the average value of the four actuator adjustment values. Moreover, the weights of f_1^e, f_2^e, f_3^e, or f_4^e must be replaced with the differences between the corresponding actuator adjustment values and the average value. Therefore, the approximation relationship can be expressed as follows:

$$\delta^e = \sum_{i=1}^{4}\left(\delta_i^e - \frac{1}{4}\sum_{j=1}^{4}\delta_j^e\right)f_i^e + \left(\frac{1}{4}\sum_{i=1}^{4}\delta_i^e\right)f_5^e. \tag{5}$$

Equation (5) is an empirical formula derived by a large number of simulations, and its correctness has been demonstrated by different simulation results. We can expand formula (5) and rewrite it in the following form

$$\delta^e = \frac{3f_1^e - f_2^e - f_3^e - f_4^e + f_5^e}{4}\delta_1^e + \frac{-f_1^e + 3f_2^e - f_3^e - f_4^e + f_5^e}{4}\delta_2^e + $$
$$\frac{-f_1^e - f_2^e + 3f_3^e - f_4^e + f_5^e}{4}\delta_3^e + \frac{-f_1^e - f_2^e - f_3^e + 3f_4^e + f_5^e}{4}\delta_4^e, \tag{6}$$
$$= \begin{bmatrix} g_1^e & g_2^e & g_3^e & g_4^e \end{bmatrix} \cdot \begin{bmatrix} \delta_1^e & \delta_2^e & \delta_3^e & \delta_4^e \end{bmatrix}^{\mathrm{T}}$$

where

$$g_1^e = \frac{3f_1^e - f_2^e - f_3^e - f_4^e + f_5^e}{4}, \tag{7a}$$

$$g_2^e = \frac{-f_1^e + 3f_2^e - f_3^e - f_4^e + f_5^e}{4}, \tag{7b}$$

$$g_3^e = \frac{-f_1^e - f_2^e + 3f_3^e - f_4^e + f_5^e}{4}, \tag{7c}$$

$$g_4^e = \frac{-f_1^e - f_2^e - f_3^e + 3f_4^e + f_5^e}{4}, \tag{7d}$$

and the superscript "T" indicates the transpose.

Equation (6) is a general expression for the point inside the eth panel. By introducing all the point coordinates of the eth panel in (6), we can obtain the following expression in the matrix form

$$\boldsymbol{\delta}^e = \begin{bmatrix} \boldsymbol{g}_1^e & \boldsymbol{g}_2^e & \boldsymbol{g}_3^e & \boldsymbol{g}_4^e \end{bmatrix}\boldsymbol{\delta}_a^e = \mathbf{G}^e\boldsymbol{\delta}_a^e, \tag{8}$$

where $\boldsymbol{\delta}_a^e = \begin{bmatrix} \delta_1^e & \delta_2^e & \delta_3^e & \delta_4^e \end{bmatrix}^{\mathrm{T}}$. The column vector $\boldsymbol{g}_1^e$ is obtained by introducing all the point coordinates of the eth panel in g_1^e, and the column vectors $\boldsymbol{g}_2^e$, $\boldsymbol{g}_3^e$, and $\boldsymbol{g}_4^e$ can be obtained in a similar manner.

To reduce the workload, the deformation functions f_1^e, f_2^e, f_3^e, f_4^e, and f_5^e for all the panels do not need to be calculated. In general, a reflector is composed of several rings, and each ring includes a lot of the same panels. Because the external loads are not considered in the derivation of the abovementioned five deformation functions, for an ideal reflector, only one panel is adopted for each ring to derive the corresponding five deformation functions, and the functions for other panels in the same ring can be directly obtained by rotating the five deformation functions along the z axis of the reflector. In this manner, one panel adjustment matrix for the entire reflector can be derived using the relationships, as shown in (8), for all the panels, to calculate the panel deformation of the entire reflector caused by adjusting all the actuators.

Assuming the adjacent actuators of two adjacent panels to be independent, the panel adjustment matrix $\mathbf{G}$ for the entire reflector can be derived using (8), and the column vector composed of all the point displacements for the entire reflector

can be expressed as

$$\boldsymbol{\delta} = \begin{bmatrix} \mathbf{G}^{(1)} & \mathbf{0} & \cdots & & & \mathbf{0} \\ \mathbf{0} & \mathbf{G}^{(2)} & & & & \\ & & \ddots & & & \vdots \\ \vdots & & & \mathbf{G}^{(e)} & & \\ & & & & \ddots & \mathbf{0} \\ \mathbf{0} & \cdots & & & \mathbf{0} & \mathbf{G}^{(M)} \end{bmatrix} \begin{bmatrix} \boldsymbol{\delta}_a^{(1)} \\ \boldsymbol{\delta}_a^{(2)} \\ \vdots \\ \boldsymbol{\delta}_a^{(e)} \\ \vdots \\ \boldsymbol{\delta}_a^{(M)} \end{bmatrix} = \mathbf{G}\boldsymbol{\delta}_{\text{actuator}}^{\text{all}}, \quad (9)$$

where M is the total number of panels, and $\boldsymbol{\delta}_{\text{actuator}}^{\text{all}}$ is a column vector composed of all the actuator adjustment values. The panel adjustment matrix $\mathbf{G}$ is a block diagonal matrix.

However, for large antennas in engineering applications, to decrease the number of actuators to reduce the cost, the adjacent corners of the adjacent panels can be supported by one actuator. In this case, the corresponding equation to (9) can be derived with the only difference pertaining to the panel adjustment matrix $\mathbf{G}$ not being a block diagonal matrix. We consider four adjacent panels as an example, as shown in Fig. 5, to describe the assembly procedure when the actuators are shared at the adjacent corners of the adjacent panels.
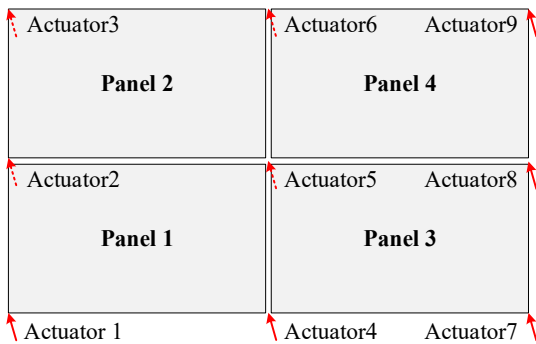

Fig. 5. Actuator distribution for the four adjacent panels.

The panel distribution and actuator serial number are shown in Fig. 5, and the corresponding equations to (6) for the four panels can be expressed as

$$\boldsymbol{\delta}^{(1)} = \begin{bmatrix} \boldsymbol{g}_1^{(1)} & \boldsymbol{g}_2^{(1)} & \boldsymbol{g}_3^{(1)} & \boldsymbol{g}_4^{(1)} \end{bmatrix} \cdot \begin{bmatrix} \delta_1 & \delta_4 & \delta_5 & \delta_2 \end{bmatrix}^{\text{T}}, \quad (10)$$

$$\boldsymbol{\delta}^{(2)} = \begin{bmatrix} \boldsymbol{g}_1^{(2)} & \boldsymbol{g}_2^{(2)} & \boldsymbol{g}_3^{(2)} & \boldsymbol{g}_4^{(2)} \end{bmatrix} \cdot \begin{bmatrix} \delta_2 & \delta_5 & \delta_6 & \delta_3 \end{bmatrix}^{\text{T}}, \quad (11)$$

$$\boldsymbol{\delta}^{(3)} = \begin{bmatrix} \boldsymbol{g}_1^{(3)} & \boldsymbol{g}_2^{(3)} & \boldsymbol{g}_3^{(3)} & \boldsymbol{g}_4^{(3)} \end{bmatrix} \cdot \begin{bmatrix} \delta_4 & \delta_7 & \delta_8 & \delta_5 \end{bmatrix}^{\text{T}}, \quad (12)$$

$$\boldsymbol{\delta}^{(4)} = \begin{bmatrix} \boldsymbol{g}_1^{(4)} & \boldsymbol{g}_2^{(4)} & \boldsymbol{g}_3^{(4)} & \boldsymbol{g}_4^{(4)} \end{bmatrix} \cdot \begin{bmatrix} \delta_5 & \delta_8 & \delta_9 & \delta_6 \end{bmatrix}^{\text{T}}, \quad (13)$$

Next, the panel adjustment matrix for the four panels can be expressed as

$$\tilde{\boldsymbol{\delta}} = \begin{bmatrix} \boldsymbol{g}_1^{(1)} & \boldsymbol{g}_4^{(1)} & \mathbf{0} & \boldsymbol{g}_2^{(1)} & \boldsymbol{g}_3^{(1)} & \mathbf{0} & \mathbf{0} & \mathbf{0} & \mathbf{0} \\ \mathbf{0} & \boldsymbol{g}_1^{(2)} & \boldsymbol{g}_4^{(2)} & \mathbf{0} & \boldsymbol{g}_2^{(2)} & \boldsymbol{g}_3^{(2)} & \mathbf{0} & \mathbf{0} & \mathbf{0} \\ \mathbf{0} & \mathbf{0} & \mathbf{0} & \boldsymbol{g}_1^{(3)} & \boldsymbol{g}_4^{(3)} & \mathbf{0} & \boldsymbol{g}_2^{(3)} & \boldsymbol{g}_3^{(3)} & \mathbf{0} \\ \mathbf{0} & \mathbf{0} & \mathbf{0} & \mathbf{0} & \boldsymbol{g}_1^{(4)} & \boldsymbol{g}_4^{(4)} & \mathbf{0} & \boldsymbol{g}_2^{(4)} & \boldsymbol{g}_3^{(4)} \end{bmatrix} \begin{bmatrix} \boldsymbol{\delta}_1 \\ \boldsymbol{\delta}_2 \\ \vdots \\ \boldsymbol{\delta}_9 \end{bmatrix} \quad (14)$$

$$= \tilde{\mathbf{G}}\tilde{\boldsymbol{\delta}}_{\text{actuator}}^{\text{all}}.$$

The panel adjustment matrix is not a block diagonal matrix and is instead a banded matrix. In the following section, the optimal actuator adjustment values are derived to minimize the reflector surface errors based on the derived panel adjustment matrix.

IV. OPTIMAL ADJUSTMENT CALCULATION

When a reflector antenna is deformed under the effects of the external loads, the reflector surface precision must be enhanced by adjusting thousands of actuators. Assuming that the column vector $\boldsymbol{d}$ is composed of the node displacements of the finite element model of the reflector and the actuator adjustment vector is $\boldsymbol{\delta}_{\text{actuator}}^{\text{all}}$, the total deformation vector $\boldsymbol{\Delta}$ can be expressed as

$$\boldsymbol{\Delta} = \boldsymbol{d} + \boldsymbol{\delta} = \boldsymbol{d} + \mathbf{G}\boldsymbol{\delta}_{\text{actuator}}^{\text{all}}. \quad (15)$$

Next, the reflector surface root mean square (rms) error after the panel adjustment can be derived as

$$rms = \sqrt{\boldsymbol{\Delta}^{\text{T}}\boldsymbol{\Delta} \Big/ N} = \sqrt{(\boldsymbol{d} + \mathbf{G}\boldsymbol{\delta}_{\text{actuator}}^{\text{all}})^{\text{T}}(\boldsymbol{d} + \mathbf{G}\boldsymbol{\delta}_{\text{actuator}}^{\text{all}}) \Big/ N}, \quad (16)$$

where N is the total number of nodes for the entire reflector.

In engineering applications, the actuator adjustment values are generally directly determined considering the normal distances between the corners of the panels of the deformed reflector and target reflector, such as the ideal reflector or best fitting reflector. However, this conventional approach is not optimal due to the panel elastic deformation. The optimal adjustment values should be derived by solving the following optimization problem:

$$\begin{aligned} &\text{Find} \quad \boldsymbol{\delta}_{\text{actuator}}^{\text{all}} \\ &\text{Min} \quad f = N \times rms^2 \\ &\text{Subject to} \quad \boldsymbol{\delta}_{\text{actuator}}^{\text{all}}\Big|_{\text{down}} \le \boldsymbol{\delta}_{\text{actuator}}^{\text{all}} \le \boldsymbol{\delta}_{\text{actuator}}^{\text{all}}\Big|^{\text{up}} \end{aligned} \quad , \quad (17)$$

where $\boldsymbol{\delta}_{\text{actuator}}^{\text{all}}\big|^{\text{up}}$ and $\boldsymbol{\delta}_{\text{actuator}}^{\text{all}}\big|_{\text{down}}$ are the upper and lower limits of the actuator adjustment values, and f is the revised objective function.

Considering that the number of actuators is extremely large, to promptly derive the optimal adjustment values, we expand the objective function f to be in the following quadratic form in the matrix form

$$f = \boldsymbol{\delta}_{\text{actuator}}^{\text{all}}{}^{\text{T}}\mathbf{G}^{\text{T}}\mathbf{G}\boldsymbol{\delta}_{\text{actuator}}^{\text{all}} + 2\boldsymbol{\delta}_{\text{actuator}}^{\text{all}}{}^{\text{T}}\mathbf{G}^{\text{T}}\boldsymbol{d} + \boldsymbol{d}^{\text{T}}\boldsymbol{d}. \quad (18)$$

Thus, the optimal solution of (17) should satisfy the following condition:

$$\frac{\partial f}{\partial \boldsymbol{\delta}_{\text{actuator}}^{\text{all}}} = 0 . \tag{19}$$

By solving (19), we can directly derive the optimal adjustment values, and the column vector can be expressed as

$$\boldsymbol{\delta}_{\text{actuator}}^{\text{all}} = -(\mathbf{G}^{\text{T}}\mathbf{G})^{-1}(\mathbf{G}^{\text{T}}\boldsymbol{d}) . \tag{20}$$

Equation (20) shows that the optimal solution of the actuator adjustment value is analytic, and thus, the computation can be easily and promptly performed. Subsequently, we can derive the total deformations after the panel adjustment by substituting (20) into (15), and the EM performance of the reflector can be easily obtained by introducing (15) and (20) into (4).

When the actuator adjustment value is positive, the panel should be moved upward; otherwise, the panel should be moved downward. The proposed method is as simple as the traditional method, and all the adjustment values can be promptly calculated through a simple matrix operation, as shown in (20). Moreover, the adjustment values are more precise compared with those calculated using the traditional method because the panel elastic deformations are considered.

Regardless of the actuators being shared at the adjacent corners of the adjacent panels, the calculation processes of the adjustment values are identical. The only difference is that the panel adjustment matrix is derived using (9) or (14) for the independent or shared actuators, respectively. In general, the difference between the deformations at the adjacent corners of the adjacent panels is small because the surface deformation is nearly continuous. Thus, to calculate the adjustment value of the shared actuator at the adjacent corners of adjacent panels, in addition to the method using (14), another simple method is to adopt the average value of the adjustment values of the independent actuators at the adjacent corners as the approximation value of that of the shared actuator.

The following section describes several simulations performed to demonstrate the correctness of the proposed method. Moreover, a comparative analysis of the proposed and traditional methods is described, and the effect of the actuator adjustment errors on the EM performance is discussed.

V. NUMERICAL RESULTS AND DISCUSSION

A. Simulation Object

To assess the performance of the proposed method, a large reflector antenna with a diameter and focal length of 35 m and 10.8 m, respectively, is adopted for the simulations. Fig. 6 shows the antenna's finite element model and panel distribution form. Nine rings of panels are supported by 10 rings of actuators, and each panel is supported by four actuators. In general, one actuator is shared at the adjacent corners of the adjacent panels

to reduce the number of actuators. For example, for the four corners at location 5 in Fig. 6, we install only one actuator to support the corners i, j, k, and m. The adjustment value of the shared actuator is approximately equal to the average value of the four adjustment values when the four independent actuators are installed at corners i, j, k, and m.

(a) Finite element model

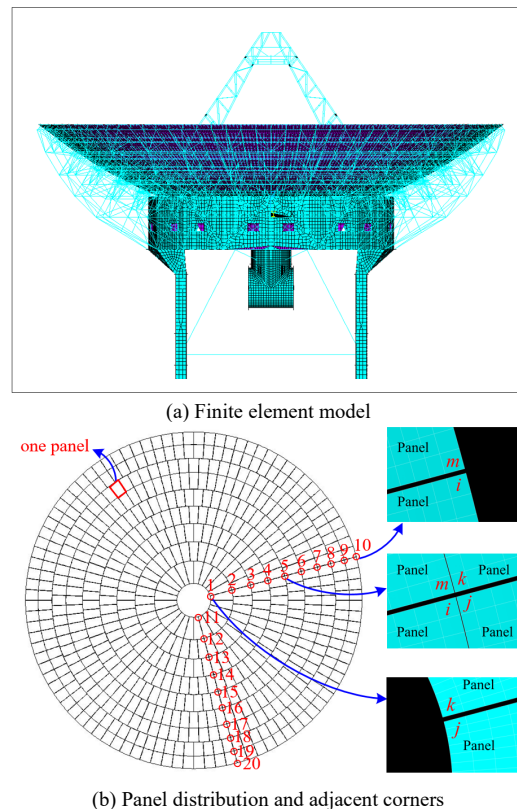

(b) Panel distribution and adjacent corners

Fig. 6. Simulation model of a 35 m reflector antenna.

First, we verify the panel adjustment matrix through the finite element simulation. Next, the actuator adjustment is calculated considering each panel to be supported by four independent actuators, and the average adjustment value of the adjacent actuators at the adjacent corners of the panels is derived. Subsequently, the surface errors and beam patterns before and after the panel adjustment are determined using the proposed approach and traditional method respectively. Finally, the effect of the actuator adjustment error on the EM performance is analyzed. The parameter P in the aperture amplitude distribution, as indicated in (2), is 1.5, and the edge taper ET is -10 dB in the EM simulations.

B. Verification of the Panel Adjustment Matrix

Consider a panel located in ring 5 as an example. The panel is supported by four actuators, and the actuator serial numbers are the same as those shown in Fig. 3. Seven cases with different adjustment values are considered, as indicated in Table I. The first five cases correspond to the typical deformations. In cases 1 and 2, one side of the panel is deformed upward, and the other side is deformed downward; in cases 3 and 4, one corner of the panel is deformed upward, and the opposite corner is deformed downward; in case 5, the entire panel is deformed upward. To

verify the generality of the panel adjustment matrix, cases 6 and 7 are also considered, which correspond to two arbitrary deformations. In the seven cases, the panel deformations caused by adjusting the actuators are calculated using two different approaches involving (1) the panel's finite element model (2) the derived panel adjustment matrix. The rms errors of the difference in the results obtained using the aforementioned two methods are presented in Table I. The results calculated using the finite element method are adopted as the references. The actuator adjustment occurs in the reflector's normal direction because the actuator is generally vertical to the panel. Considering that the z axial deformations exert the most notable effects on the reflector's EM performance, only the z axial deformations are adopted to calculate the rms errors.

TABLE I
SEVEN SIMULATION CASES WITH DIFFERENT ADJUSTMENT VALUES

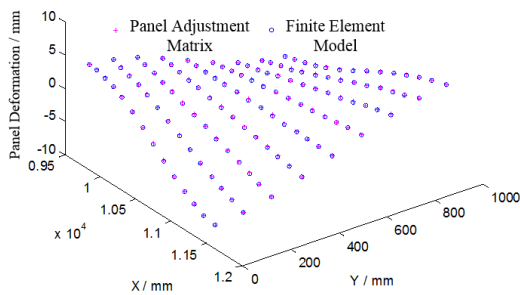| Cases	1	2	3	4	5	6	7
Actuator 1/mm	5	-5	-5	5	5	6	10
Actuator 2/mm	5	-5	0	0	5	-8	8
Actuator 3/mm	-5	5	5	-5	5	2	4
Actuator 4/mm	-5	5	0	0	5	-4	6
rms error/μm	26	26	26	26	96	52	128

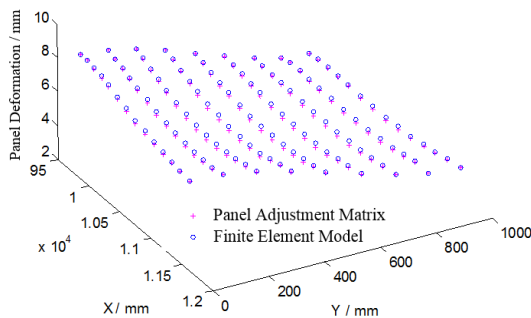Fig. 7. Panel deformations for case 6.

Fig. 8. Panel deformations for case 7.

The rms errors for the first four cases are extremely small, close to 0.026 mm. Case 5 shows that the rms error increases when the actuator adjustments are in the same directions, which can also be verified by the result for case 7. Case 6 shows that when the actuator adjustments are in different directions, the rms error becomes relatively small, owing to which, the first four cases involve small rms errors. Figs. 7 and 8 present the panel deformations for cases 6 and 7, respectively, and it can be noted that the two deformations calculated using the two methods are in agreement, and the errors in the center area are slightly larger

than those in the edge region. Anyway, the results presented in Table I and Figs. 7 and 8 show that the approximation error of the panel adjustment matrix is very small.

C. Comparison Before and After Adjustment

Considering only the gravity deformation, several simulations are performed to enhance the EM performance of the 35 m reflector antenna by adjusting the actuators. Because the gravity deformation at a given tilt angle can be expressed as a weighted sum of the deformations at the horizon and zenith positions [37], only the following two cases are considered: (1) pointing skyward; (2) pointing horizontally. The corresponding actuator adjustment values are calculated using two methods, specifically, (1) the traditional method and (2) the proposed method. In the traditional method, the adjustment value is determined by the projection of the distance between the panel corner of the deformed reflector and that of the ideal reflector in the axis direction of the actuator. In the proposed method, the adjustment values are derived using (20). To obtain the optimal panel adjustments, the surface errors of the reflector after the panel adjustment can be derived, and the rms errors can be obtained easily.

Table II lists the reflector's surface rms errors for different methods, and Figs. 9 and 10 present the corresponding surface error distributions when the reflector points skyward and horizontally, respectively. When the reflector points skyward, under the effect of gravity, the rms error is 1.333 mm before adjustment, and after the panel adjustment, the rms errors are reduced to 0.284 mm and 0.067 mm for the traditional method and proposed method, respectively. Although both the methods exhibit a reasonable performance, the precision of the proposed method is higher than that of the traditional method, and the proposed method is approximately 4.24 times more accurate. When the reflector points horizontally, similar results are obtained, and the proposed method is approximately 5.55 times more accurate.
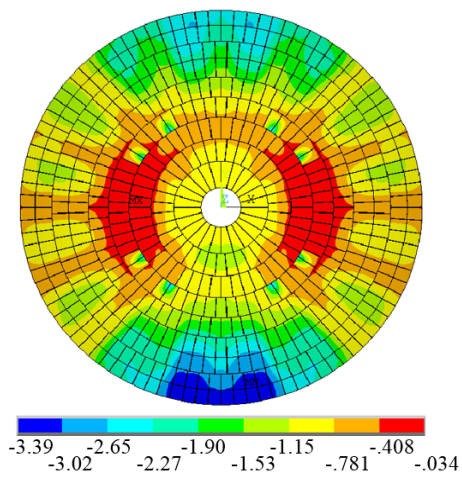
In general, the motion resolution of the actuator applied in the large millimeter or submillimeter wave reflector in engineering applications can reach a few microns. Thus, the rms error can be further reduced from 0.284 mm to 0.067 mm or from 0.283 mm to 0.051 mm, as indicated in Table II, when the proposed method is adopted. Compared with the surface precision after panel adjustment, the adjustment error caused by the motion resolution of a few microns is extremely small and does not considerably influence the surface precision.

TABLE II
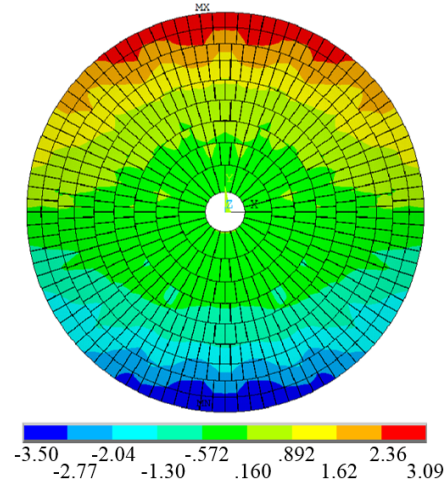RMS ERRORS OF THE REFLECTOR SURFACE BEFORE AND AFTER ADJUSTMENT

Terms [a]	Pointing skywards			Pointing horizontally		
	B-A	T-M	P-M	B-A	T-M	P-M
rms error/mm	1.333	0.284	0.067	1.269	0.283	0.051

[a] B-A, T-M, and P-M denote before adjustment, traditional method, and proposed method, respectively, and the same abbreviations hold in other tables.
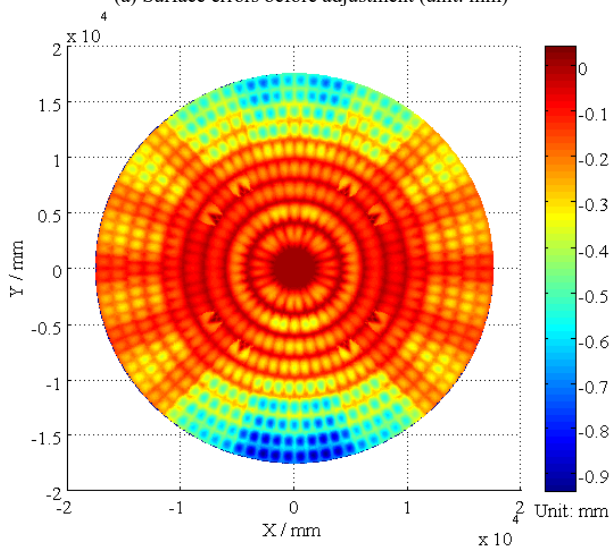
(a) Surface errors before adjustment (unit: mm)

(b) Surface errors after adjustment using the traditional method

(c) Surface errors after adjustment using the proposed method

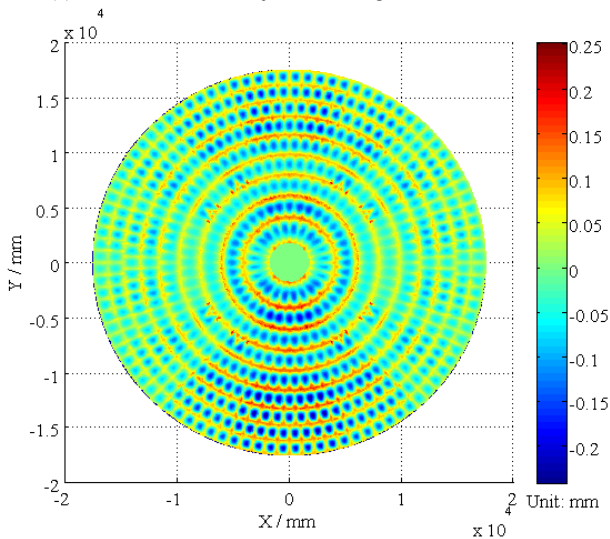Fig. 9. Surface error distributions when the reflector points skyward.

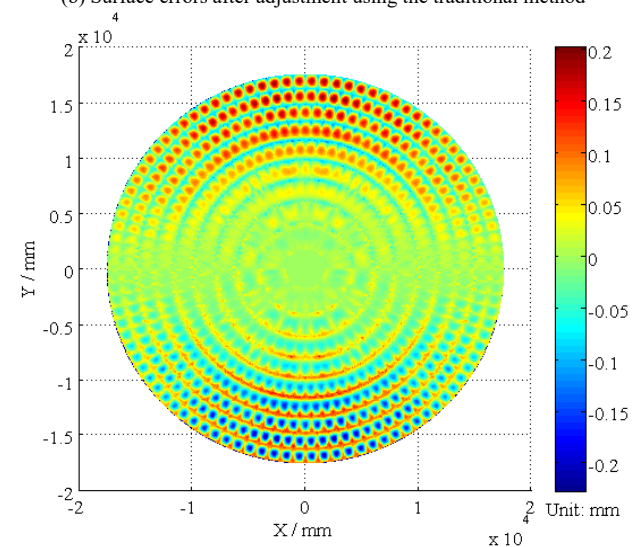(a) Surface errors before adjustment (unit: mm)

(b) Surface errors after adjustment using the traditional method

(c) Surface errors after adjustment using the proposed method

Fig. 10. Surface error distributions when the reflector points horizontally.

Next, the surface error distributions are discussed. Figs. 9(a) and 9(b) show the surface error distributions before the adjustment and after the adjustment using the traditional method. Although the surface errors are considerably reduced, the error distribution is slightly similar to that before the adjustment. As shown in Fig. 9(a), the deformations are always negative when the reflector points skyward. Thus, the actuator adjustment values are always positive when the reflector points skyward. In the traditional method, when the panel corners are adjusted to the positions of the vertices of the panels of the ideal reflector, the panel elastic deformation is not considered, which is always negative when the reflector points skyward. Thus, the surface errors after the adjustment through the traditional method are always negative, as shown in Fig. 9(b). Moreover, the axis directions of the actuators do not coincide with the displacement vectors of the panel vertices, and thus, the panel vertices of the deformed reflector cannot be moved to the ideal locations completely. At the same time, the axis directions of the actuators of the deformed reflector antennas are unknown, and thus, the ideal axis directions for the ideal reflector antenna are adopted in the process of the calculation of the adjustment values, and certain some adjustment errors remain. As shown in Fig. 9(b), the errors at the panel corners do not become zero, especially for the panels in the uppermost and lowermost regions with large deformations. Thus, the actuator adjustment values are not the optimal solution derived using the traditional method. Fig. 9(c) shows the surface error distribution when the proposed method is adopted. The surface error distribution is more uniform than that when the traditional method is adopted. According to Fig. 9(c), for each panel after the adjustment, certain positive and negative errors exist, indicating that the deformed panels have been adjusted to the optimal locations.

Fig. 10 shows the surface error distributions for the case in which the reflector points horizontally. Similar results as those shown in Fig. 9 can be attained. The error distribution shown in Fig. 10(c) is more uniform than that shown in Fig. 10(b), because the panel elastic deformations are considered in the derived panel adjustment matrix, which indicates a high approximation precision, as clearly illustrated in Figs. 7 and 8.

Next, we demonstrate that the average value of the actuator adjustments at the adjacent corners of the adjacent panels can be approximately adopted as the adjustment amount of the shared actuator when only one actuator is installed to support the adjacent two or four corners. When the reflector points skyward, as shown in Fig. 9(a), for the first ten adjustment points in Fig. 6, the average value can be calculated by

$$\delta_{\text{shared}} = (\delta_i + \delta_j + \delta_k + \delta_m)/4 , \qquad (21)$$

where, δ_i, δ_j, δ_m, and δ_k are the adjustment values of the actuators at corners i, j, k, and m, respectively, and the adjustment values are listed in Table III. When the reflector points horizontally, the corresponding values for the last ten adjustment points in Fig. 6 are listed in Table IV. For the adjacent corners, the two or four adjustment values are nearly identical, and the max percentage error relative to the average value is less than 6%, except for that of the twelfth adjustment point. The reason for the large percentage error for the twelfth

adjustment point is the relatively small adjustment value. The absolute value of the error is extremely small, and thus, it does not considerably influence the EM performance. Therefore, for the reflector with the shared actuator at the adjacent corners, in addition to the method in which the adjustment value of the shared actuator can be directly calculated using (14) and (20), another simple method is to consider the average value of the independent actuator adjustment amounts calculated using (9) and (20) as the approximation adjustment value of the shared actuator. The patterns for these two methods nearly coincide and are not presented here due to the space limitation.

TABLE III
AVERAGE ACTUATOR ADJUSTMENTS AT THE ADJACENT CORNERS OF ADJACENT PANELS WHEN THE REFLECTOR POINTS SKYWARD

Terms [a]	δ_i /mm	δ_j /mm	δ_k /mm	δ_m /mm	Aver /mm	|Max| /mm	Perc /%
1	\	1.122	1.114	\	1.118	0.004	0.36
2	1.102	1.162	1.177	1.090	1.133	0.044	3.88
3	0.332	0.298	0.301	0.327	0.315	0.018	5.71
4	0.235	0.223	0.232	0.246	0.234	0.012	5.13
5	0.276	0.257	0.263	0.272	0.267	0.010	3.75
6	1.054	1.013	0.995	1.037	1.025	0.030	2.93
7	1.495	1.429	1.397	1.459	1.445	0.050	3.46
8	1.511	1.465	1.435	1.476	1.472	0.039	2.65
9	1.547	1.549	1.527	1.517	1.535	0.018	1.17
10	1.222	\	\	1.212	1.217	0.005	0.41

[a] "Aver", "|Max|", and "Perc" denote the average value, maximum absolute error, and percentage error, respectively.

TABLE IV
AVERAGE ACTUATOR ADJUSTMENTS AT THE ADJACENT CORNERS OF ADJACENT PANELS WHEN THE REFLECTOR POINTS HORIZONTALLY
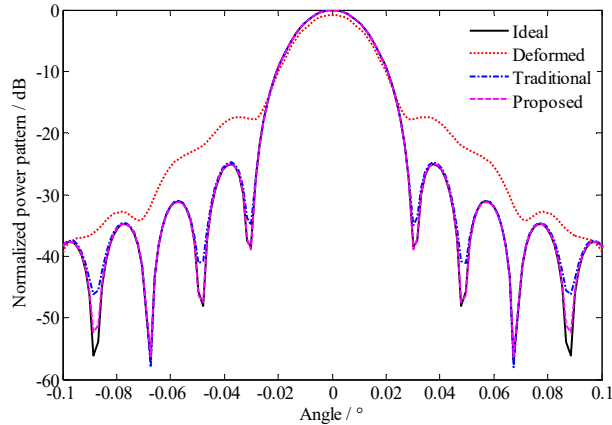
Terms	δ_i /mm	δ_j /mm	δ_k /mm	δ_m /mm	Aver /mm	|Max| /mm	Perc /%
11	\	-0.172	-0.162	\	-0.167	0.005	2.99
12	0.143	0.186	0.178	0.138	0.161	0.024	15.5
13	0.418	0.445	0.432	0.401	0.424	0.023	5.42
14	0.551	0.568	0.556	0.552	0.557	0.011	1.97
15	0.858	0.880	0.875	0.882	0.874	0.016	1.83
16	1.497	1.525	1.516	1.505	1.511	0.014	0.93
17	2.512	2.490	2.491	2.451	2.486	0.035	1.41
18	3.213	3.191	3.173	3.226	3.201	0.028	0.87
19	4.064	4.114	4.073	4.028	4.070	0.044	1.08
20	4.453	\	\	4.431	4.442	0.011	0.25

Based on the reflectors with the surface errors, as shown in Figs. 9 and 10, the corresponding power patterns are determined through (4) considering an operating frequency of 24 GHz. Figs. 11 and 12 present the power patterns of the reflectors in Figs. 9 and 10, respectively. For each reflector, the patterns in the horizontal and vertical planes are determined. The gain loss and first sidelobe level increment (SLLI) for each pattern are presented in Tables V and VI for the reflectors in Figs. 9 and 10, respectively.
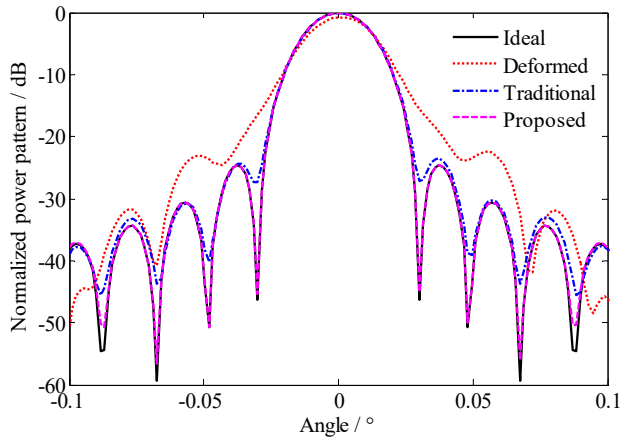
When the reflector points skyward, under the effect of the gravity deformations, as indicated in Table V, the gain losses are 0.804 dB and 0.789 dB for the patterns in the horizontal and vertical planes, respectively. After the panel adjustment through the traditional method, the two gain losses are reduced to 0.044 dB. When the proposed method is adopted, the two gain losses are reduced to 0.013 dB. When the reflector points horizontally, as shown in Table VI, when using the traditional

method, in the horizontal and vertical planes, the gain loss is reduced to 0.121 dB from 2.27 dB and to 0.028 dB from 0.244 dB, respectively. When using the proposed method, the gain losses in the horizontal and vertical planes are reduced to 0.005 dB. Both the traditional and proposed methods lead to an improvement; however, the gain loss is considerably smaller when the adjustment is performed using the proposed method.
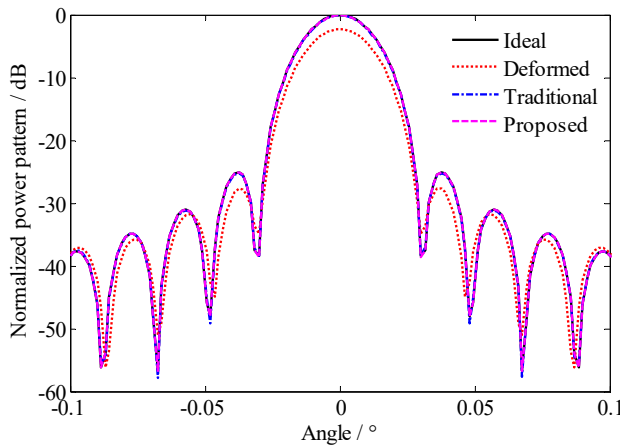

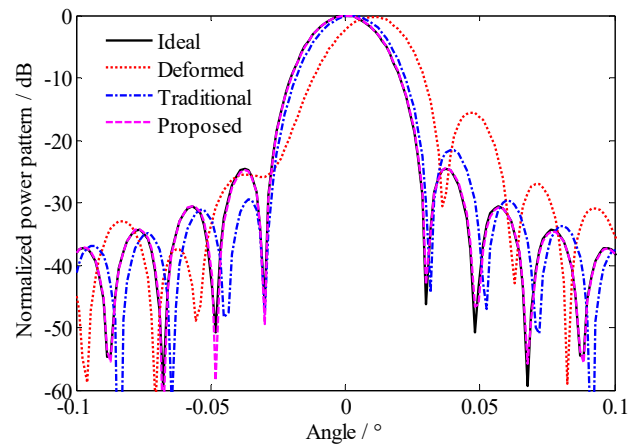(a) Patterns in the horizontal plane

(b) Patterns in the vertical plane

Fig. 11. Patterns of the reflectors in Figure 9 when the reflector points skyward.

(a) Patterns in the horizontal plane

(b) Patterns in the vertical plane

Fig. 12. Patterns of the reflectors in Figure 10 when the reflector points horizontally.

TABLE V
GAIN LOSS AND SLLI FOR EACH PATTERN IN FIGURE 11

Terms [a]	Horizontal plane			Vertical plane		
	B-A	T-M	P-M	B-A	T-M	P-M
Gain loss/dB	0.804	0.044	0.013	0.789	0.044	0.013
L-1st SLLI/dB	8.53	0.41	0.09	/	0.13	-0.01
R-1st SLLI/dB	8.53	0.41	0.09	/	1.04	0.01

[a] L-1st SLLI and R-1st SLLI indicate the first sidelobe level increment in the left and right sides, respectively.

TABLE VI
GAIN LOSS AND SLLI FOR EACH PATTERN IN FIGURE 12

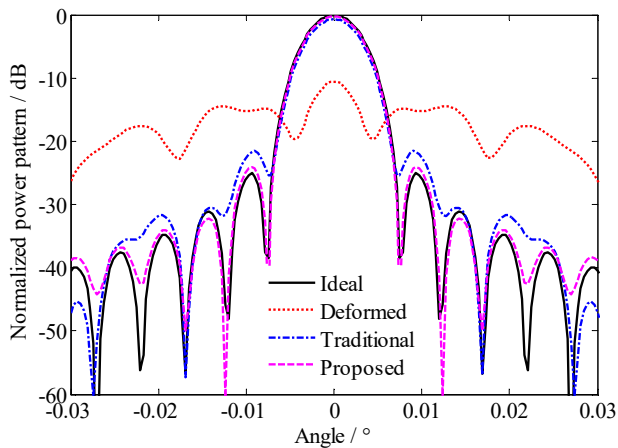| Terms [a]	Horizontal plane			Vertical plane		
	B-A	T-M	P-M	B-A	T-M	P-M
Gain loss/dB	2.27	0.121	0.005	0.244	0.028	0.005
L-1st SLLI/dB	-0.37	0.01	0.01	-0.7	-4.84	-0.16
R-1st SLLI/dB	-0.36	0.01	0.01	9.42	3.06	0.09
P-E/arc second	/	/	/	37.8	10.8	0

[a] P-E denotes the pointing error.

The patterns shown in Figs. 11 and 12 indicate that the SLLs after the panel adjustment are nearly identical to the ideal patterns, and the proposed method exhibits a higher agreement, especially for the patterns shown in Figs. 11(b) and 12(b), in which the SLLI is more notable due to the existence of the pointing errors.
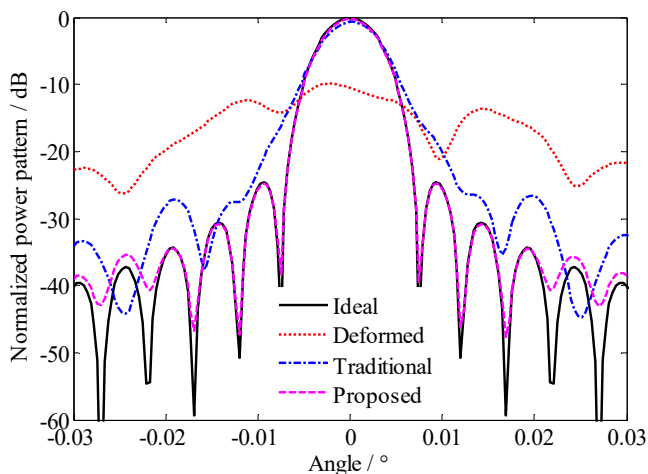
To consider the pointing error, Fig. 12(b) is considered as an example. The pointing error is 37.8 arcsec for the deformed reflector before the panel adjustment, and it is reduced to 10.8 arcsec while the traditional method is adopted. When the proposed method is applied, the pointing error is nearly zero. The effect of the proposed method is more pronounced compared with that of the traditional method. Thus, next, the proposed method is applied to the panel adjustment of the deformed reflector with a higher operation frequency because the pattern is more sensitive to the surface deformation.

The operating frequency of 96 GHz is selected for the reflectors with the surface error distributions when the reflector points skyward, as shown in Fig. 9. The patterns are plotted in

Fig. 13, and the gain loss and first SLLI for each pattern are indicated in Table VII. Fig. 13 shows that the patterns of the deformed reflectors are considerably worse before the panel adjustment because the operation frequency is higher, and the advantage of the proposed method is more pronounced than that of the traditional method. The gain loss is further reduced from 0.701 dB to 0.208 dB, and the SLLs are notably improved when the proposed method is adopted. In other words, the correctness and effectiveness of the proposed method are clearly demonstrated by the simulations.

(a) Patterns in the horizontal plane

(b) Patterns in the vertical plane

Fig. 13. Patterns of the reflectors shown in Figure 9 when the reflector points skyward with an operation frequency of 96 GHz.

TABLE VII
GAIN LOSS AND SLLI FOR EACH PATTERN SHOWN IN FIGURE 13

Terms	Horizontal plane		Vertical plane	
	T-M	P-M	T-M	P-M
Gain loss/dB	0.701	0.208	0.701	0.208
L-1st SLLI/dB	4.231	1.298	/	0.208
R-1st SLLI/dB	4.181	1.308	/	0.248

D. Effect Analysis of the Actuator Adjustment Errors

The effect of the actuator adjustment error on the EM performance for the 35 m reflector antenna with an operating

frequency of 12 GHz is examined through the Monte Carlo method by using the proposed panel adjustment matrix. Assuming that the actuator adjustment error follows a normal distribution with a zero mean and standard deviation τ, ten thousand kinds of different adjustment errors for all the actuators are generated in MATLAB, and the corresponding patterns are calculated to derive the average gain loss and first SLL. The parameter P is 1.5, and ET is -10 dB in the aperture amplitude distribution, as indicated in (2). Table VIII lists six cases with different standard deviations of the adjustment errors, along with the corresponding average surface rms errors, average gain losses, and average first SLLs. The surface rms error caused by the actuator adjustment errors is approximately 0.6τ.

TABLE VIII
SIX SIMULATION CASES AND SIMULATION RESULTS

τ /mm	0.5	1.0	1.5	2.0	2.5	3.0
τ/λ	0.02	0.04	0.06	0.08	0.1	0.12
rms/mm	0.3	0.6	0.9	1.2	1.5	1.8
rms/λ	0.012	0.024	0.036	0.048	0.06	0.072
Gain loss/dB	0.065	0.254	0.577	1.004	1.568	2.201
1st SLL/dB	-24.97	-24.64	-23.98	-23.42	-22.56	-21.96

Fig. 14 shows the variation curves of the gain loss and the first SLL versus the standard deviation of the actuator adjustment errors. The gain loss becomes increasingly large, and the first SLL rises increasingly high with the increase in the adjustment errors. The detailed values are listed in Table VIII. For example, when the gain loss is required to be less than 0.254 dB, the standard deviation of the actuator adjustment errors should be less than 0.04λ. Using the curves shown in Fig. 14, we can determine the actuator adjustment accuracy according to the EM performance requirement.
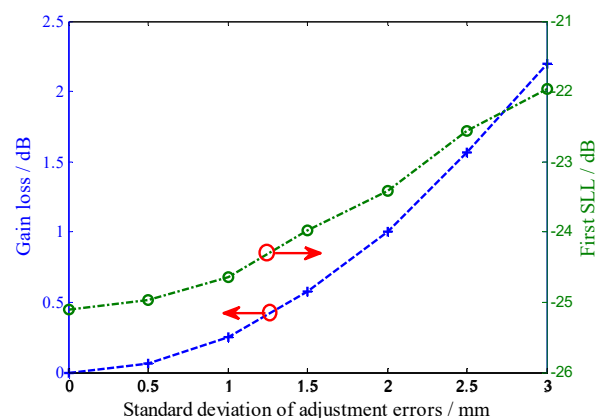

Fig. 14. Gain losses and first SLLs for the six different cases listed in Table VIII.

Next, the adjustment errors for each ring of the actuators are considered. Overall, there exist ten rings of the actuators, and we assume that the adjustment errors only exist in one ring of the actuators for each simulation. The relevant effects on the gain and first SLL are analyzed for the different standard deviations of the adjustment errors. Figs. 15 and 16 present the effects on the gain and first SLL, respectively.

For the active main reflector shown in Fig. 6, Fig. 15 shows that the adjustment errors of the third and fourth actuators most notably influence the reflector's gain, and the effects become increasingly large with the increase in the adjustment errors. Fig. 16 shows the effects on the first SLL, and it can be noted that the effects on the first SLL and gain are considerably different. The adjustment errors of the first three rings of the actuators increase the first SLL, whereas the errors of the other actuators decrease the first SLL. The actuator adjustment errors in rings 1, 2, 5, and 6 exert the most notable influence, and the adjustment errors in rings 4, 9, and 10 only slightly influence the first SLL. Specifically, the adjustment errors exert different effects on the different SLLs, and the comprehensive effect analysis of the adjustment errors of the different rings of the actuators on the EM performance and the detailed sensitivity analysis must be performed in the future work. Moreover, the effects of the adjustment errors on the mian beam and SLLs are also dependent on the aperture amplitude distribution and the ratio of focal length to diameter. Considering Figs. 15 and 16, we can determine a reasonable distribution of the adjustment errors according to the requirements of the gain loss and first SLL.

Fig. 15. Gain losses caused by the adjustment errors of the different rings of actuators

Fig. 16. First SLLs caused by the adjustment errors of the different rings of actuators.

VI. CONCLUSION

This paper presents a new method to calculate the actuator adjustment values of an active main reflector antenna with a large aperture and high frequency. In this approach, the panel elastic deformation is considered, and a panel adjustment matrix is established, based on which, a calculation equation for the actuator adjustment value is derived. Several simulations are performed, which demonstrate the correctness and effectiveness of the proposed method. Compared with the traditional method, the proposed method exhibits a higher adjustment accuracy, and the calculation procedure is a simple matrix operation, which is suitable for use in engineering applications to enhance the EM performance of large aperture and high frequency reflector antenna. The effects of the actuator adjustment errors on the reflector's gain and SLL are analyzed through the Monte Carlo method, and several interesting results are obtained. Using the derived variation characteristics of the gain loss and SLL, a reasonable distribution of the actuators with different adjustment accuracies can be obtained. In engineering applications, the proposed method can be directly applied to calculate the adjustment values of the actuators for the active main reflector, and the simulation results can provide valuable guidance for the design and adjustment of the actuator system.

REFERENCES

[1] Y. Rahmat-Samii and R. Haupt, "Reflector antenna developments: a perspective on the past, present, and future," *IEEE Antennas Propag. Mag.*, vol. 57, no. 2, pp. 85–95, April 2015.

[2] Jacob W. M. Baars and Hans J. Karcher., "Seventy years of radio telescope design and construction," *URSI Radio Science Bulletin*, vol. 2017, no. 362, pp.15-38, Sept. 2017.

[3] S. Von Hoemer and W. Wong, "Gravitational deformation and astigmatism of tiltable radio telescopes," *IEEE Trans. Antennas Propag.*, vol. 23, no. 5, pp. 689-695, Sept. 1975.

[4] A. Greve and M. Bremer., "Thermal design and thermal behaviour of radio telescopes and their enclosures," Springer, 2010.

[5] N. Ukita, H. Ezawa, B. Ikenoue, and M. Saito, "Thermal and wind effects on the azimuth axis tilt of the ASTE 10-m antenna," *Publications of the National Astronomical Observatory of Japan*, vol. 10, pp: 25-33, 2017.

[6] B. Y. Duan and C. S. Wang, "Reflector antenna distortion analysis using MEFCM," *IEEE Trans. Antennas Propag.*, vol. 57, no.10, pp. 3409- 3413, 2009.

[7] S. F. Feng, C. S. Wang, B. Y. Duan, and Y. Ban., "Design of tipping structure for 110 m high-precision radio telescope," *Acta Astronaut.*, vol. 141, pp. 50–56, Dec. 2017.

[8] C. S. Wang, B. Y. Duan, and Y. Y. Qiu, "On distorted surface analysis and multidisciplinary structural optimization of large reflector antennas," *Structural and Multidisciplinary Optimization*, vol. 33, no. 6, pp. 519-528, June 2007.

[9] Hans J. Karcher and Jacob W. M. Baars, "Ideas for future large single dish radio telescopes," *Proc. of SPIE*, vol. 9145, pp. 914503-1-11, 2014.

[10] F. P. Schloerb, D. Sanchez, G. Narayanan, N. Erickson, K. Souccar, G. Wilson, D. Gale, D. H. Hughes, and D. Smith, "Calibration and Operation of the Active Surface of the Large Millimeter Telescope," *Proc. of SPIE*, vol. 9906, pp. 99066C-1-7, 2016.

[11] B. Nikolic, R. E. Hills, and J. S. Richer, "Measurement of antenna surfaces from in- and out-of-focus beam maps using astronomical sources," *Astronomy and Astrophysics*, vol. 465, no. 2, pp. 679-683, 2007.

[12] J. A. Martinez-Lorenzo, C. M. Rappaport, and A. G. Pino., "Reflector antenna distortion determination: An iterative-field-matrix solution," *Radio Science*, vol. 43, no. 4, Aug. 2008.

[13] C. S. Wang, H. H. Li, K. Ying, Q. Xu, N. Wang, B. Y. Duan, W. Gao, L. Xiao, and Y. H. Duan, "Active surface compensation for large radio telescope antennas," *International Journal of Antennas and Propagation*, vol. 2018, pp. 3903412-1-17, March 2018.
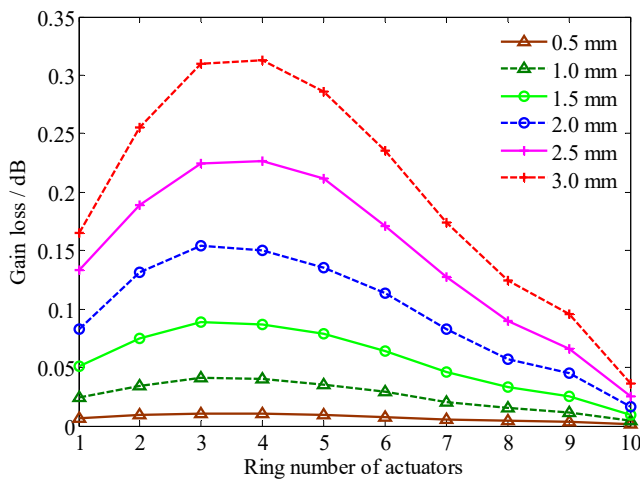
This article has been accepted for publication in a future issue of this journal, but has not been fully edited. Content may change prior to final publication. Citation information: DOI 10.1109/TAP.2021.3069493, IEEE Transactions on Antennas and Propagation

> REPLACE THIS LINE WITH YOUR PAPER IDENTIFICATION NUMBER (DOUBLE-CLICK HERE TO EDIT) <   13

[14] P. Y. Lian, C. S. Wang, S. Xue, Xu Q., Y. Shi, Y. Jia, B. B. Xiang, Y. Wang, and Y. F. Yan, "Surface Adjustment Strategy for A Large Radio Telescope with Adjustable Dual Reflectors," *IET Microw. Antennas Propag.*, vol. 13, no.15, pp. 2669-2677, Dec. 2019.

[15] W. Wang, C. S. Wang, B. Y. Duan, G. J. Leng, and X. P. Li, "Compensation for gravity deformation via subreflector motion of 65 m shaped Cassegrain antenna," *IET Microw. Antennas Propag.*, vol. 8, no. 3, pp. 158-164, Feb. 2014.

[16] A. Greve and M. Bremer, "Improvement of the IRAM 30-m telescope from temperature measurements and finite-element calculations," *IEEE Transactions on Antennas and Propagation*, vol. 53, no. 2, pp. 851-860, Feb. 2005.

[17] B. B. Xiang, C. S. Wang, P. Y. Lian, N. Wang, and Y. Ban, "Optimal subreflector position determination of shaped dual-reflector antennas based on the parameters iteration approach," *Research in Astronomy and Astrophysics*, vol. 19, no. 4, pp. 6201-6210, 2019.

[18] C. S. Wang, L. Xiao, W. Wang, Q. Xu, B. B. Xiang, J. F. Zhong, L. Jiang, H. Bao, and N. Wang, "An adjustment method for active reflector of large high-frequency antennas considering gain and boresight," *Research in Astronomy and Astrophysics*, vol. 17, no. 5, pp. 4301-4312, 2017.

[19] W. Wang, B. Y. Duan, P. Li, and L. W. Song, "Optimal surface adjustment by the error transformation matrix for a segmented reflector antenna," *IEEE Antennas Propag Mag.*, vol. 52, no. 3, pp. 80-88, June 2010.

[20] P. Bolli, L. Olmi, J. Roda, and G. Zacchiroli, "A novel application of the active surface of the shaped Sardinia radio telescope for primary-focus operation," *IEEE Antennas and Wireless Propagation Letters*, vol. 13, pp. 1713-1716, Aug. 2014.

[21] S. F. Feng, Y. Ban, B. Y. Duan, C. S. Wang, and B. Wang, "Electronic performance-oriented mold sharing method and application in QTT 110 m large radio telescope," *IEEE Trans. Antennas Propag.*, vol. 68, no. 8, pp. 6407-6412, Aug. 2020.

[22] Y. Rahmat-Samii, "An efficient computational method for characterizing the effects of random surface errors on the average power pattern of reflectors," *IEEE Trans. Antennas Propag.*, vol. 31, no.1, pp. 92-98, Jan. 1983.

[23] S. Sinton and Y. Rahmat-Samii, "Random surface error effects on offset cylindrical reflector antennas," *IEEE Trans. Antennas Propag.*, vol. 51, no. 6, pp. 1331-1337, June 2003.

[24] M. Wang, W. Wang, C. S. Wang, and J. Z. Zhou, "A practical approach to evaluate the effects of machining errors on the electrical performance of reflector antennas based on paneled forms," *IEEE Antennas and Wireless Propagation Letters*, vol. 13, no. 1, pp. 1341-1344, July 2014.

[25] P. Y. Lian, B. Y. Duan, W. Wang, B. B. Xiang, and N. G. Hu, "Effects of Non-uniform Surface Errors along the Radius on Reflector's Radiation Characteristic and Its Quality Evaluation," *IEEE Trans. Antennas Propagat.*, vol. 63, no. 5, pp. 2312-2316, May 2015.

[26] A. Greve, D. Morris, J. Penalver, C. Thum, and M. Bremer, "The beam pattern of reflector antennas with buckled panels," *IEEE Transactions on Antennas and Propagation*, vol. 58, no. 3, pp. 959-962, Mar. 2010.

[27] P. Rocca, N. Anselmi, and A. Massa, "Interval arithmetic for pattern tolerance analysis of parabolic reflectors," *IEEE Trans. Antennas Propag.*, vol. 62, no. 10, pp. 4952-4960, Oct. 2014.

[28] N. Anselmi, M. Salucci, P. Rocca, and A. Massa, "Generalised interval-based analysis tool for pattern distortions in reflector antennas with bump-like surface deformations," IET Microwaves Antennas & Propagation, vol. 10, no. 9, pp. 909-916, 2016.

[29] N. Anselmi, L. Manica, P. Rocca, and Andrea Massa, "Tolerance analysis of antenna arrays through interval arithmetic," IEEE Transactions on Antennas and Propagation, vol. 61, no. 11, pp. 5496-5507, Nov. 2013.

[30] L. Tenuti, N. Anselmi, P. Rocca, M. Salucci, and A. Massa, "Minkowski sum method for planar arrays sensitivity analysis with uncertain-but-bounded excitation tolerances," IEEE Transactions on Antennas and Propagation, vol. 65, no. 1, pp. 167-177, 2017.

[31] W. T. Smith and R. J. Bastian, "An approximation of the radiation integral for distorted reflector antennas using surface-error decomposition," *IEEE Antennas Wireless Propag. Lett.*, vol. 45, no. 1, pp. 5-10, Jan. 1997.

[32] P. Y. Lian, B. Y. Duan, W. Wang, C. S. Wang, S. X. Zhang, and B. B. Xiang, "A Pattern Approximation Method for Distorted Reflector Antennas Using Piecewise Linear Fitting of the Exponential Error Term," *IEEE Trans. Antennas Propag.*, vol. 63, no. 10, pp. 4546-4551, Oct. 2015

[33] S. X. Zhang, B. Y. Duan, G. G. Yang, Y. L. Zong, and Y. Q. Zhang, "An approximation of pattern analysis for distorted reflector antennas using structural-electromagnetic coupling model," *IEEE Trans. Antennas Propag.*, vol. 61, no. 9, pp. 4844–4847, Sep. 2013.

[34] J. Dong, W. Y. Zhong, J. Q. Wang, Q. H. Liu, Z. Q. Shen, "Correcting gravitational deformation at the Tianma radio telescope," *IEEE Trans. Antennas Propag.*, vol. 66, no. 4, pp. 2044-2048, April 2018.

[35] P. Li, B. Y. Duan, W. Wang, and F. Zheng, "Electromechanical coupling analysis of ground reflector antennas under solar radiation," *IEEE Antennas and Propagation Magazine*, vol. 54, no. 5, pp. 40-57, Oct. 2012.

[36] J. Zhang, J. Huang, J. Zhou, C. S. Wang, and Y. Zhu, "A compensator for large antennas based on pointing error estimation under a wind load," *IEEE Trans. Antennas Propag.*, vol. 25, no. 5, pp. 1912-1920, Sept. 2017.

[37] S. F. Feng, B. Y. Duan, C. S. Wang, Y. Ban, and W. Wang, "Novel Worst-Case Surface Accuracy Evaluation Method and Its Application in Reflector Antenna Structure Design," IEEE Access, vol. 7, pp. 140328-140335, Sep. 2019.

Peiyuan Lian was born in 1989. He received his B.S. and Ph.D. degrees in electromechanical engineering from School of Mechano-Electronic Engineering, Xidian University, Xi'an, China, in 2011 and 2017, respectively. He is currently a lecturer at the School of Mechano-Electronic Engineering, Xidian University. His current major research interests focus on structural-electromagnetic analysis, optimization design, and thermal analysis of large reflector antennas and phased array antennas.

Congsi Wang was born in 1980. He received his B.S., M.S., and Ph.D. degrees in electromechanical engineering from Xidian University, Xi'an, China, in 2001, 2004, and 2007, respectively. He is currently a professor of Electromechanical Engineering, Key Laboratory of Electronic Equipment Structure of Ministry of Education, Vice Director of Institute of Mechatronics, Vice President of School of Mechano-Electronic Engineering, Xidian University. From 2009 to 2011, he served as a Postdoctoral Fellow at Nanjing Research Institute of Electronics Technology (NRIET), Nanjing, China. From 2012 to 2013, he is a Visiting Scholar at University of California, Berkeley. His research interests are primarily in the area of electromechanical coupling of electronic equipment with emphasis on the modeling, influencing mechanism, design of structural-electromagnetic-thermal coupling of antennas including phased array antennas, reflector antennas, and deployable antennas.

Song Xue was born in 1986. He completed his Bachelor of Science from the Hefei University of Technology in 2009, his Master of Science from the Dalian University of Technology, China in 2012 and in 2016, a Ph.D. degree from the Curtin University, Australia, in the area of condition monitoring of the mechanical system. In 2018, he was appointed as a Lecturer in the School of Mechano-Electronic Engineering, Xidian University, Xi'an, Shannxi, China. His current academic and research interest has focused on the modeling and signal processing for the system fault detection as well as mechatronics system reliability analysis.

Qian Xu was born in 1981. He received his B.S. in mechanic engineering and automation from Huazhong University of Science and Technology, Wuhan, China, in 2004, and then he received his M.S. in instrument science and technology in 2008 and Ph.D. degrees in radio physics in 2011 from Wuhan University, Wuhan, China. He is currently a professor senior engineer of the Xinjiang Astronomical Observation, Chinese Academy of Sciences, Urumqi, China. His major research interests include optimization design of reflector antenna, effect analysis of environmental loads, deformation compensation, antenna control.

Na Wang was born in 1965. She is now Deputy Director of National Astronomical Observatories, Chinese Academy of Sciences, Director of Xinjiang Astronomical Observatory, Chinese Academy of Sciences, Member of the Party Committee, National Candidate of New Century Talents Project, and PhD Supervisor. Her research interests include Radio Astronomy, Related Technology of Large Aperture Radio Telescope.

Binbin Xiang was born in 1986. He received his B.S. and M.S. degrees in electromechanical engineering from Xidian University, Xi'an, China, in 2008 and 2012, respectively. Since 2012, he has been with the Xinjiang Astronomical Observation, Chinese Academy of Sciences, Urumqi, China. He is currently pursuing the Ph.D. degree at the School of Mechanical-Electrical Engineering, Xidian University. His major research interests include integrated structural-electromagnetic analysis and structure optimization design of reflector antennas.

Yu Shi is currently a Senior Lecturer in Mechanical Engineering at the University of Chester and leads the Chester Smart Composite Group. He has research interests and experience in simulation and non-destructive damage investigation of composites, lamb wave propagation in composites, and integration of composites for energy harvesting. He graduated PhD from the University of Sheffield and then joined the Energy Harvesting group at the University of Exeter as a research fellow. Following that, he worked for Advanced Forming Research Centre (AFRC) to model metal work piece forming/forging process for project from Rolls Royce.

Yu Jia is currently a Senior Lecturer in Mechanical Engineering at Aston University. He received a First Class in MEng Electromechanical Engineering from the University of Southampton in 2010, and PhD in Engineering from the University of Cambridge in 2014. He was then a Research Associate at Cambridge for a year. He is a co-founder of power Ltd and a steering board member of the Energy Harvesting Network. His research interests include vibration energy harvesting, micro-electromechanical systems, nonlinear vibration dynamics and smart integrated systems.